

# Coupled finite element/boundary element formulation for scattering from axially-symmetric objects in three dimensions

Ahmad T. Abawi<sup>a)</sup>

Heat, Light, and Sound Research, Inc., 12625 High Bluff Drive, Suite 211, San Diego, California 92130, USA

Petr Krysl

University of California, San Diego, 9500 Gilman Drive #0085, La Jolla, California 92093, USA

(Received 14 August 2017; revised 2 November 2017; accepted 12 November 2017; published online 18 December 2017)

The fluid-structure interaction technique provides a paradigm for solving scattering from elastic structures embedded in an environment characterized by a Green's function, by a combination of finite and boundary element methods. In this technique, the finite element method is used to discretize the equations of motion for the structure and the Helmholtz-Kirchhoff integral with the appropriate Green's function is used to produce the discrete pressure field in the exterior medium. The two systems of equations are coupled at the surface of the structure by imposing the continuity of pressure and normal particle velocity. The present method condenses the finite element model so that finally only the boundary element problem needs to be solved. This results in a significant reduction in the number of unknowns and hence a much lower cost. In this paper, the fluid-structure interaction method is specialized to axially-symmetric objects for non-axially-symmetric loading in free space using a circumferential Fourier expansion of the fields. The specialization of the method to axially-symmetric objects results in even further significant reductions in computation. The method is validated using well-known benchmark solutions. A derivation of the method for an arbitrarily-shaped elastic structure embedded in an arbitrary environment characterized by a Green's function is given in the Appendix. © 2017 Acoustical Society of America.

<https://doi.org/10.1121/1.5016030>

[ANN]

Pages: 3637–3648

## I. INTRODUCTION

The problem of determining the interaction between a submerged elastic structure and its surrounding fluid is of considerable interest, particularly in underwater acoustics and aeronautics where it is required to determine the acoustic field about an arbitrary three-dimensional (3D) structure. While the standard method of a solution for an arbitrary elastic structure is the finite element method, the solution of the reduced wave equation in the surrounding medium is best handled by the boundary integral equation, as it replaces the infinite domain problem by an integral over the surface of the submerged structure. Furthermore, the boundary integral method has the advantage of reducing the dimensionality of the problem by one. In contrast, the finite element method is not well-suited for solving the wave equation in the surrounding fluid environment due to difficulty in satisfying the radiation condition as well as due to the demands on the mesh size and the difficulty in generating the fluid mesh.

For these reasons, the problem of fluid-structure interaction is perhaps best treated by a combination of the finite element method to model the motion of the structure and the boundary integral method to model the acoustic field in its surrounding medium, where the coupling between the two models is achieved by imposing the continuity of pressure and normal particle velocity at the surface of the structure. The coupled finite and boundary integral method has been

used by several authors in recent years<sup>1,2</sup> (also see Amini *et al.*<sup>3</sup> and the references therein). A good review of the method is given recently by Ref. 4. The main differences in these approaches are the particular finite element package and boundary integral formulation employed, the numerical approximation used, and the details of the method of coupling.

In this paper, we specialize the fluid-structure interaction method to axially-symmetric objects in three dimensions ensconced by a non-axially-symmetric incident field.<sup>5</sup> In the surrounding fluid, the axial symmetry of the structure allows for the incident field to be expanded in a circumferential Fourier series, essentially reducing a 3D problem into a series of two-dimensional (2D) problems, one for each circumferential order. Application of such a model was first shown by Wilson in static stress analysis.<sup>6</sup> A textbook account of such a technique (in a different setting) has been given by Zienkiewicz.<sup>7</sup> More recently, Winnicki and Zienkiewicz<sup>8</sup> showed this procedure to be an efficient alternative to a 3D analysis for nonlinear viscoplastic analysis; Spilker and Daugirda<sup>9</sup> expanded the method in the context of hybrid finite element methods; Carter and Booker<sup>10</sup> studied soil consolidation; Danielson and Tielking,<sup>11</sup> Kaiser *et al.*,<sup>12</sup> and Kukudzhanov and Shneiderman<sup>13</sup> applied the technique to nonlinear static analysis. In the present work, this technique is expanded to include the case of free vibrations.

This paper is organized in the following way: In Sec. II the fluid-structure interaction method is derived for axially-symmetric structures with a general 3D response. In Sec. III,

<sup>a)</sup>Electronic mail: [abawi@hlsresearch.com](mailto:abawi@hlsresearch.com)

the boundary element equations for a vibrating axially-symmetric structure are derived. In Sec. IV the model is applied to compute scattering from a solid steel sphere, an aluminum spherical shell, and a hemispherical boss and the results are compared with analytical solutions. To demonstrate the speed of the model, it is used to compute the back-scattered target strength as a function of aspect angle and frequency for an aluminum cylinder and the results are compared with those obtained by a finite element model designed for axially-symmetric objects.<sup>14</sup> This is followed by concluding remarks in Sec. V.

## II. THE FLUID-STRUCTURE FORMULATION FOR AXIALLY-SYMMETRIC STRUCTURES IN THREE DIMENSIONS

The derivation of the fluid-structure formulation for an axially-symmetric object in three dimensions is based on an analogous formulation for an arbitrarily shaped elastic structure. Since the former derivation relies heavily on the notation used in the latter, we include the derivation for an arbitrary structure in the Appendix for convenience and completeness.

The analysis of axially-symmetric structures under non-axially-symmetric loading can be effectively carried out within the context of semi-analytic techniques. We consider here an axially-symmetric 3D structure whose material properties are independent of the circumferential coordinate direction. Contrariwise, the applied load may depend on this coordinate. The technique expresses the variation of the load and the field variables in the circumferential coordinate in the form of a Fourier series, thus reducing the 3D analysis to a relatively small number of uncoupled 2D analyses. Provided that the loading may be represented by a reasonable number of harmonics, the semi-analytic procedure will be more efficient than a full 3D analysis.

The displacement vector is written in the coordinate system  $r, z, \theta$  as

$$\begin{bmatrix} u_r(r, z, \theta) \\ u_z(r, z, \theta) \\ u_\theta(r, z, \theta) \end{bmatrix} = \sum_{\ell=0,1,\dots} \left\{ \left[ \mathbf{C}_\ell^{(s)} \right] \sum_{i=1}^N N_i(r, z) \left[ \mathbf{U}_{i\ell}^{(s)} \right] + \left[ \mathbf{C}_\ell^{(a)} \right] \sum_{i=1}^N N_i(r, z) \left[ \mathbf{U}_{i\ell}^{(a)} \right] \right\}, \quad (1)$$

where  $N_i(r, z)$  is the basis function in the plane of the cross-section,  $[\mathbf{U}_{i\ell}^{(s)}]$  and  $[\mathbf{U}_{i\ell}^{(a)}]$  are vectors of the nodal displacements at node  $i$  for the expansion terms symmetric with respect to  $\theta=0$  displayed with the superscript  $(s)$  [or anti-symmetric with respect to  $\theta=0$ , indicated with a superscript  $(a)$ ],

$$\left[ \mathbf{U}_{i\ell}^{(s)} \right] = \begin{bmatrix} u_{ir} \\ u_{iz} \\ u_{i\theta} \end{bmatrix}^{(s)}, \quad \left[ \mathbf{U}_{i\ell}^{(a)} \right] = \begin{bmatrix} u_{ir} \\ u_{iz} \\ u_{i\theta} \end{bmatrix}^{(a)} \quad (2)$$

and the circumferential expansion coefficients expressed by the matrices

$$\left[ \mathbf{C}_\ell^{(s)} \right] = \begin{bmatrix} \cos(\ell\theta) & 0 & 0 \\ 0 & \cos(\ell\theta) & 0 \\ 0 & 0 & -\sin(\ell\theta) \end{bmatrix}, \quad \left[ \mathbf{C}_\ell^{(a)} \right] = \begin{bmatrix} \sin(\ell\theta) & 0 & 0 \\ 0 & \sin(\ell\theta) & 0 \\ 0 & 0 & \cos(\ell\theta) \end{bmatrix}, \quad (3)$$

with the same meaning of the superscripts. Here  $\ell$  refers to the circumferential Fourier mode.

In the cylindrical coordinate system,  $\mathcal{B}$  is the symmetric-gradient operator

$$\mathcal{B} = \begin{bmatrix} \frac{\partial}{\partial r} & 0 & 0 \\ 0 & \frac{\partial}{\partial z} & 0 \\ \frac{1}{r} & 0 & \frac{1}{r} \frac{\partial}{\partial \theta} \\ \frac{\partial}{\partial z} & \frac{\partial}{\partial r} & 0 \\ \frac{1}{r} \frac{\partial}{\partial \theta} & 0 & \frac{\partial}{\partial r} - \frac{1}{r} \\ 0 & \frac{1}{r} \frac{\partial}{\partial \theta} & \frac{\partial}{\partial z} \end{bmatrix}, \quad (4)$$

to yield the strain components  $[\epsilon] = [\epsilon_r, \epsilon_z, \epsilon_\theta, \epsilon_{rz}, \epsilon_{r\theta}, \epsilon_{z\theta}]$  defined as

$$\begin{aligned} \epsilon_r &= \frac{\partial u_r}{\partial r}, & \epsilon_z &= \frac{\partial u_z}{\partial z}, & \epsilon_\theta &= \frac{u_r}{r} + \frac{1}{r} \frac{\partial u_\theta}{\partial \theta}, \\ \epsilon_{rz} &= \frac{\partial u_r}{\partial z} + \frac{\partial u_z}{\partial r}, & \epsilon_{r\theta} &= \frac{1}{r} \frac{\partial u_r}{\partial \theta} + \frac{\partial u_\theta}{\partial r} - \frac{u_\theta}{r}, \\ \epsilon_{z\theta} &= \frac{1}{r} \frac{\partial u_z}{\partial \theta} + \frac{\partial u_\theta}{\partial z}. \end{aligned} \quad (5)$$

The basis functions  $N_i(r, z)$  are generated on a mesh of the cross-section, either quadrilateral or triangular. In this work, we use ordinary isoparametric elements of linear order of approximation.

Application of the differential operator, Eq. (4), to the displacement vector, Eq. (1), yields the expression for the strain vector

$$[\epsilon] = \sum_{\ell=0,1,\dots} \left\{ \left[ \mathcal{A}_\ell^{(s)} \right] \sum_{i=1}^N \left[ \mathcal{B}_i \right] \left[ \mathbf{U}_{i\ell}^{(s)} \right] + \left[ \mathcal{A}_\ell^{(a)} \right] \sum_{i=1}^N \left[ \mathcal{B}_i \right] \left[ \mathbf{U}_{i\ell}^{(a)} \right] \right\}, \quad (6)$$

where we introduce the matrices

$$[\mathcal{A}_\ell^{(s)}] = \begin{bmatrix} \cos(\ell\theta) & 0 & 0 & 0 & 0 & 0 \\ 0 & \cos(\ell\theta) & 0 & 0 & 0 & 0 \\ 0 & 0 & \cos(\ell\theta) & 0 & 0 & 0 \\ 0 & 0 & 0 & \cos(\ell\theta) & 0 & 0 \\ 0 & 0 & 0 & 0 & \sin(\ell\theta) & 0 \\ 0 & 0 & 0 & 0 & 0 & \sin(\ell\theta) \end{bmatrix} \quad (7)$$

and

$$[\mathcal{A}_\ell^{(a)}] = \begin{bmatrix} \sin(\ell\theta) & 0 & 0 & 0 & 0 & 0 \\ 0 & \sin(\ell\theta) & 0 & 0 & 0 & 0 \\ 0 & 0 & \sin(\ell\theta) & 0 & 0 & 0 \\ 0 & 0 & 0 & \sin(\ell\theta) & 0 & 0 \\ 0 & 0 & 0 & 0 & -\cos(\ell\theta) & 0 \\ 0 & 0 & 0 & 0 & 0 & -\cos(\ell\theta) \end{bmatrix}, \quad (8)$$

and the nodal strain-displacement matrix (compare with the 3D version [Eq. (A2)])

$$[\mathcal{B}_i] = \begin{bmatrix} \partial N_i / \partial r & 0 & 0 \\ 0 & \partial N_i / \partial z & 0 \\ N_i / r & 0 & -\ell N_i / r \\ \partial N_i / \partial z & \partial N_i / \partial r & 0 \\ -\ell N_i / r & 0 & (N_i / r - \partial N_i / \partial r) \\ 0 & -\ell N_i / r & -\partial N_i / \partial z \end{bmatrix}. \quad (9)$$

The notation in this section resembles that of Spilker and Daugrida<sup>9</sup> except that the particular order  $r, z, \theta$  in which the cylindrical coordinates and the corresponding unknowns are arranged has been changed such that the coordinates in the plane of the generating section are first and the circumferential coordinate is last.

For easy reference we list here the weighted residual equation

$$-\omega^2 \int_{D_-} \delta \mathbf{u}^T \rho_f \mathbf{u} \, dV + \int_{D_-} \delta \mathbf{u}^T \mathcal{B}^T \mathbf{D} \mathcal{B} \mathbf{u} \, dV + \int_S \delta \mathbf{u}^T \mathbf{p} \mathbf{n} \, dS = 0. \quad (10)$$

The details can be found in the [Appendix](#) where this equation is discussed as Eq. (A1). The integral over the volume in Eq. (10) is separated into integration over the cross-section and integration in the angular coordinate. So, for the first term in Eq. (10) we obtain

$$-\omega^2 \int_{D_-} \delta \mathbf{u}^T \rho_f \mathbf{u} \, dV = -\omega^2 \int_A \int_0^{2\pi} \delta \mathbf{u}^T \rho_f \mathbf{u} \, d\theta \, dA, \quad (11)$$

where  $dA$  is the cross-sectional area element. Upon substitution we find that the unlike (symmetric with anti-symmetric)

products  $[\mathbf{C}_\ell^{(s)}][\mathbf{C}_\ell^{(a)}]$  integrate to zero in the circumferential direction due to the identity

$$\int_0^{2\pi} \sin(\ell\theta) \cos(m\theta) \, d\theta = 0. \quad (12)$$

For the integrals of like terms we have

$$I_c(\ell, m) = \int_0^{2\pi} \cos(\ell\theta) \cos(m\theta) \, d\theta = \begin{cases} 2\pi, & \text{for } \ell = m = 0; \\ \pi, & \text{for } \ell = m \geq 1; \\ 0, & \text{otherwise} \end{cases} \quad (13)$$

$$I_s(\ell, m) = \int_0^{2\pi} \sin(\ell\theta) \sin(m\theta) \, d\theta = \begin{cases} \pi, & \text{for } \ell = m \geq 1; \\ 0, & \text{otherwise} \end{cases} \quad (14)$$

and therefore for the circumferential mode number  $\ell$  the  $3 \times 3$  contributions to the mass matrix  $\mathbf{M}_\ell^{(s)}$ , coupling nodes  $i, k$  are

$$\mathbf{M}_{ik\ell}^{(s)} = \begin{bmatrix} I_c(\ell, \ell) & 0 & 0 \\ 0 & I_c(\ell, \ell) & 0 \\ 0 & 0 & I_s(\ell, \ell) \end{bmatrix} \int_S N_i \rho_f N_k \, dA, \quad (15)$$

for the symmetric terms and

$$\mathbf{M}_{ik\ell}^{(a)} = \begin{bmatrix} I_s(\ell, \ell) & 0 & 0 \\ 0 & I_s(\ell, \ell) & 0 \\ 0 & 0 & I_c(\ell, \ell) \end{bmatrix} \int_S N_i \rho_f N_k \, dA, \quad (16)$$

for the anti-symmetric terms  $\mathbf{M}_\ell^{(a)}$ .

Here we consider only homogeneous isotropic solids with the material stiffness matrix of the form

$$\mathbf{D} = \begin{bmatrix} \lambda + 2G & \lambda & \lambda & 0 & 0 & 0 \\ \lambda & \lambda + 2G & \lambda & 0 & 0 & 0 \\ \lambda & \lambda & \lambda + 2G & 0 & 0 & 0 \\ 0 & 0 & 0 & G & 0 & 0 \\ 0 & 0 & 0 & 0 & G & 0 \\ 0 & 0 & 0 & 0 & 0 & G \end{bmatrix}, \quad (17)$$

where we introduce the Lamé constant

$$\lambda = \frac{E\nu}{(1+\nu)(1-2\nu)}, \quad (18)$$

with  $E$  as the Young's modulus,  $\nu$  as the Poisson ratio, and  $G$  as the shear modulus. Extension of this formulation to suitably anisotropic materials (such as composites) is possible.

The second term in the weighted residual equation, Eq. (10), is then expanded as follows: For the number of circumferential modes  $\ell$  and  $m$  and node numbers  $j$  and  $i$  we obtain

$$\left[ \delta \mathbf{U}_{i\ell}^{(s)} \right]^T \int_{D_-} [\mathcal{B}_i]^T [\mathcal{A}_\ell^{(s)}] \mathbf{D} [\mathcal{A}_m^{(s)}] [\mathcal{B}_j] dV \left[ \mathbf{U}_{jm}^{(s)} \right], \quad (19)$$

for the symmetric terms, which allows us to define a submatrix of the stiffness matrix  $\mathbf{K}_\ell^{(s)}$  for the symmetric modes that couples nodes  $j$  and  $i$ ,

$$\mathbf{K}_{ij\ell}^{(s)} = \int_{D_-} [\mathcal{B}_i]^T [\mathcal{A}_\ell^{(s)}] \mathbf{D} [\mathcal{A}_m^{(s)}] [\mathcal{B}_j] dV. \quad (20)$$

The submatrix of the stiffness matrix  $\mathbf{K}_\ell^{(a)}$  for the anti-symmetric terms follows analogously by replacing  $[\mathcal{A}_\ell^{(s)}]$  with  $[\mathcal{A}_\ell^{(a)}]$  and so on. The result will be non-zero only for  $\ell = m$ . This can be shown by considering the products

$$\left[ \mathcal{A}_\ell^{(s)} \right] \mathbf{D} \left[ \mathcal{A}_m^{(s)} \right], \quad (21)$$

where the block structure of the material stiffness matrix together with the special structure of the  $[\mathcal{A}_\ell^{(s)}]$  matrices ensure that the integrals in the circumferential direction still satisfy the relationships described by the symbols  $I_c(\ell, m)$  and  $I_s(\ell, m)$ . A similar result is derived for the product with two anti-symmetric terms.

Analogously, the unlike products

$$\left[ \mathcal{A}_\ell^{(s)} \right] \mathbf{D} \left[ \mathcal{A}_m^{(a)} \right] \quad (22)$$

(and similar) will all vanish when integrated in the circumferential direction. Since the symmetric and anti-symmetric terms decouple, the equation of motion of the structure in matrix form [which for the 3D setting is given in the Appendix as Eq. (A5)] is written separately for the symmetric and anti-symmetric terms of the circumferential expansion as

$$(-\omega^2 \mathbf{M}_\ell^{(s)} + \mathbf{K}_\ell^{(s)}) \mathbf{U}_\ell^{(s)} = \mathbf{F}_\ell^{(s)} \quad (23)$$

and

$$(-\omega^2 \mathbf{M}_\ell^{(a)} + \mathbf{K}_\ell^{(a)}) \mathbf{U}_\ell^{(a)} = \mathbf{F}_\ell^{(a)}. \quad (24)$$

Here  $\ell$  is the number of the circumferential mode, and the symmetric mass matrix is composed of the sub-matrices [Eq. (15)], and the anti-symmetric mass matrix is composed of sub-matrices [Eq. (16)]. The symmetric stiffness matrix is composed of sub-matrices [Eq. (20)] and the anti-symmetric stiffness matrix is obtained analogously.

We assume the total pressure in the fluid surrounding the structure to be expanded in symmetric and anti-symmetric terms as

$$p = \sum_{\ell=0,1,\dots} p_\ell^{(s)} \cos(\ell\theta) + \sum_{\ell=1,2,\dots} p_\ell^{(a)} \sin(\ell\theta). \quad (25)$$

The loading vectors are obtained from the expression for the 3D case given in the Appendix as Eq. (A8) by substitution of the expansion (25).

### A. Coupling of the boundary element and axially-symmetric finite element models

The coupling of the axially-symmetric finite element model with the Fourier circumferential expansion and the boundary element model is shown in the discrete form.

When the expansion [Eq. (25)] is introduced in the third term of the weighted residual equation, Eq. (10), the resulting products of sines and cosines from  $\delta \mathbf{u} p$  will result in the  $3 \times 1$  coupling submatrix

$$\mathbf{L}_{\ell Kq}^{(s)} = \int_{\Gamma_q} N_K \begin{bmatrix} I_c(\ell, \ell) & 0 & 0 \\ 0 & I_c(\ell, \ell) & 0 \\ 0 & 0 & 0 \end{bmatrix} \mathbf{nd}\Gamma_q, \quad (26)$$

for symmetric terms of the circumferential mode  $\ell$  to couple the pressure degree of freedom  $q$  with the displacement degrees of freedom at node  $K$ ;  $\Gamma_q$  is the line segment in the generating section in the  $rz$  plane associated with the pressure degree of freedom  $q$ , and  $d\Gamma$  is an element of the boundary curve. For the anti-symmetric terms we obtain

$$\mathbf{L}_{\ell Kq}^{(a)} = \int_{\Gamma_q} N_K \begin{bmatrix} I_s(\ell, \ell) & 0 & 0 \\ 0 & I_s(\ell, \ell) & 0 \\ 0 & 0 & 0 \end{bmatrix} \mathbf{nd}\Gamma_q. \quad (27)$$

The discrete symmetric and anti-symmetric forces acting on the surface of the solid due to the total pressure in the fluid are then written as

$$\mathbf{F}_\ell^{(s,a)} = -\mathbf{L}_\ell^{(s,a)} \mathbf{P}_\ell^{(s,a)}, \quad (28)$$

where  $\mathbf{P}$  is the vector of the total pressure values at the line segments at the boundary of the cross-section exposed to the fluid.

The mean normal velocity in the boundary element method (BEM), piecewise constant along the surface panels, can be expressed from the vector of the finite element (FE) nodal velocities as shown below, where a submatrix of the matrix  $\mathbf{L}'$ ,

$$\mathbf{L}'_{qK} = \left( \int_{S_q} d\Gamma_q \right)^{-1} \int_{\Gamma_q} N_K \mathbf{n}^T dS_q, \quad (29)$$

couples the mean normal velocity on the surface panel  $q$  to the velocity of node  $K$ . The discrete form of the relationship of the normal velocities at the boundary line segments and the velocity of the nodes on the boundary of the structure follows as

$$\mathbf{V}_n = \mathbf{L}' \mathbf{V}. \quad (30)$$

The velocity of the structure can be expressed at steady state through the displacement, and that can be obtained from the equation of motion if the loads on the surface are known (refer to the [Appendix](#) for details). From Eq. (29), we can write

$$\mathbf{V}_\ell^{(s,a)} = -i\omega \mathbf{D}^{-1} \mathbf{L}_\ell^{T(s,a)} \mathbf{U}^{(s,a)}, \quad (31)$$

for each circumferential order. Combining Eqs. (23), (24), (28), and (31), we obtain

$$\mathbf{V}_\ell^{(s,a)} = i\omega \mathbf{D}^{-1} \mathbf{L}_\ell^{T(s,a)} (-\omega^2 \mathbf{M}_\ell^{(s,a)} + \mathbf{K}_\ell^{(s,a)})^{-1} \mathbf{L}_\ell^{(s,a)} \mathbf{P}_\ell^{(s,a)}. \quad (32)$$

This is the axially-symmetric counterpart of Eq. (A20). In Sec. III, we derive equations for the radiated field of a vibrating structure in its surrounding fluid medium.

## B. Boundary conditions for the structural equations

Even when the scatterer is unsupported (free-floating), the axially-symmetric 3D formulation requires the imposition of some boundary conditions to guarantee that the displacement field remains continuous:

- (1) For the higher circumferential modes,  $\ell \neq 0$ , the constraint  $u_z = 0$  needs to be enforced for all nodes located on the axis of symmetry.
- (2) For the fundamental circumferential modes,  $\ell = 0$ , we require the following:
  - (a) For the symmetric case: The constraint  $u_\theta = 0$  needs to be enforced at all nodes, and the constraint  $u_r = 0$  needs to be enforced for all nodes located on the axis of symmetry.
  - (b) For the anti-symmetric case: The constraint  $u_r = u_z = 0$  needs to be enforced at all nodes, and the constraint  $u_\theta = 0$  needs to be enforced for all nodes located on the axis of symmetry.

## III. THE FIELD OF A VIBRATING AXIALLY-SYMMETRIC STRUCTURE

For an acoustic wave,  $p_{\text{inc}}(\mathbf{x})$ , incident on the structure, resulting in a scattered acoustic wave,  $p_{\text{scat}}(\mathbf{x})$ , the integral equation for the total acoustic wave,  $p(\mathbf{x}) = p_{\text{inc}}(\mathbf{x}) + p_{\text{scat}}(\mathbf{x})$ , is given by

$$\begin{aligned} & \int \left( p(\mathbf{x}') \frac{\partial G(\mathbf{x}, \mathbf{x}')}{\partial \mathbf{n}'} + i\omega \rho_f v_n(\mathbf{x}') G(\mathbf{x}, \mathbf{x}') \right) dS' \\ & = \begin{cases} p(\mathbf{x}) - p_{\text{inc}}(\mathbf{x}), & \mathbf{x} \in V_+, \\ \frac{1}{2} p(\mathbf{x}) - p_{\text{inc}}(\mathbf{x}), & \mathbf{x} \in S, \\ -p_{\text{inc}}(\mathbf{x}), & \mathbf{x} \in V_-, \end{cases} \end{aligned} \quad (33)$$

where  $\mathbf{x}$  denotes the field coordinates and  $\mathbf{x}'$  denotes the source coordinates (surface of the scatterer),  $dS'$  is the surface area element,  $V_-$  denotes the space in  $\mathcal{R}^3$  occupied by the deformable structure with closed surface  $S$ , and  $V_+$  denotes the unbounded fluid region exterior to  $S$  with density  $\rho_f$  and sound speed  $c$ , and where the gradient of the total pressure is expressed in terms of the normal surface velocity of the vibrating surface (positive into the acoustic fluid). To obtain the solution in the surrounding fluid, we substitute Eq. (25) into the middle equation in Eq. (33), to get

$$\begin{aligned} & \frac{1}{2} \sum_{\ell=0}^{\infty} \left[ p_\ell^{(s)}(r, z) \cos \ell\theta + p_\ell^{(a)}(r, z) \sin \ell\theta \right] \\ & - \sum_{\ell=0}^{\infty} \int_{S'} \left[ p_\ell^{(s)}(r', z') \cos \ell\theta' + p_\ell^{(a)}(r', z') \sin \ell\theta' \right] \\ & \quad \times \frac{\partial G(\mathbf{x}, \mathbf{x}')}{\partial \mathbf{n}'} dS' \\ & = -i\omega \rho \sum_{\ell=0}^{\infty} \int_{S'} \left[ v_\ell^{(s)}(r', z') \cos \ell\theta' + v_\ell^{(a)}(r', z') \sin \ell\theta' \right] \\ & \quad \times G(\mathbf{x}, \mathbf{x}') dS' + p_{\text{inc}}(\mathbf{x}), \end{aligned} \quad (34)$$

where a similar expansion as in Eq. (25) has been used for the normal velocity,  $v$ . To facilitate the derivation of the axially-symmetric equations, refer to Fig. 1. Applying the integral operator

$$\int_0^{2\pi} \cos m\theta d\theta, \quad (35)$$

to the above equation results in

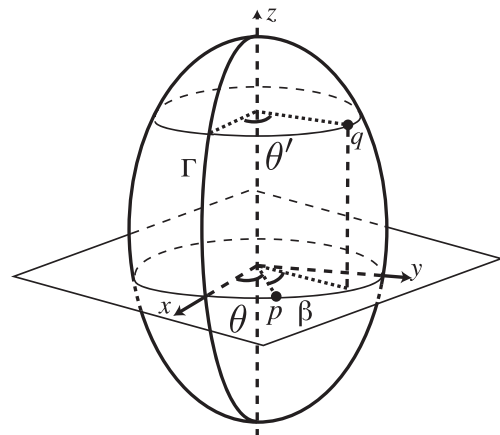


FIG. 1. The geometry used in deriving the axially-symmetric equations.

$$\begin{aligned}
& \frac{1}{2} \sum_{\ell=0}^{\infty} \int_0^{2\pi} p_{\ell}^{(s)}(r, z) \cos \ell \theta \cos m \theta \, d\theta \\
& - \sum_{\ell=0}^{\infty} \int_0^{2\pi} \int_{S'} p_{\ell}^{(s)}(r', z') \cos \ell \theta' \cos m \theta \, d\theta \frac{\partial G(\mathbf{x}, \mathbf{x}')}{\partial n'} \, dS' \\
& = -i\omega\rho \sum_{\ell=0}^{\infty} \int_0^{2\pi} \int_{S'} v_{\ell}^{(s)}(r', z') \cos \ell \theta' \cos m \theta \, d\theta \\
& \quad \times G(\mathbf{x}, \mathbf{x}') \, dS' + \int_0^{2\pi} p_{\text{inc}}(\mathbf{x}) \cos m \theta \, d\theta, \tag{36}
\end{aligned}$$

where Eq. (12) has been used. It can be shown that in free space, where the free space Green's functions  $G(\mathbf{x}, \mathbf{x}')$  is a function of the difference of the angles  $\beta = (\theta - \theta')$ , there is no contribution from the off-diagonal terms ( $\ell \neq m$ ) in Eq. (36). For a general environment (not free space), the contribution from the off-diagonal terms results in the coupling of coefficients of various circumferential orders, resulting in a numerically-intensive system of coupled equations, which negates the numerical advantages offered by an axially-symmetric formulation. For this reason, the rest of this formulation is specialized to free space. Writing  $dS' = r' d\theta' d\Gamma'$ , where  $\Gamma$  is the generating curve shown in Fig. 1, we get for  $\ell = m$ ,

$$\begin{aligned}
& \frac{1}{2} \epsilon \pi p_m^{(s)}(r, z) - \frac{1}{2} \int_0^{2\pi} \int_0^{2\pi} \int_{\Gamma'} p_m^{(s)}(r', z') (\cos m(\theta' - \theta) \\
& \quad + \cos m(\theta' + \theta)) \frac{\partial G(\mathbf{x}, \mathbf{x}')}{\partial n'} r' \, d\Gamma' \, d\theta \, d\theta' \\
& = \frac{-i\omega\rho}{2} \int_0^{2\pi} \int_0^{2\pi} \int_{\Gamma'} v_m^{(s)}(r', z') (\cos m(\theta' - \theta) \\
& \quad + \cos m(\theta' + \theta)) G(\mathbf{x}, \mathbf{x}') r' \, d\Gamma' \, d\theta \, d\theta' + p_m^{\text{inc}(s)}(r, z), \tag{37}
\end{aligned}$$

where  $\epsilon = 2$  for  $m = 0$  and  $\epsilon = 1$  otherwise. In deriving Eq. (37) use has been made of the identity

$$\cos m\theta' \cos m\theta = \frac{1}{2} (\cos m(\theta' - \theta) + \cos m(\theta' + \theta)), \tag{38}$$

and Eq. (13) has been used to get its first term. The last term in Eq. (37) is defined as

$$p_m^{\text{inc}(s)}(r, z) = \int_0^{2\pi} p_{\text{inc}}(\mathbf{x}) \cos m\theta \, d\theta. \tag{39}$$

For  $m = 0$ , Eq. (37) becomes

$$\begin{aligned}
& \frac{1}{2} p_0^{(s)}(r, z) - \frac{1}{2\pi} \int_0^{2\pi} \int_0^{2\pi} \int_{\Gamma'} p_0^{(s)}(r', z') \frac{\partial G(\mathbf{x}, \mathbf{x}')}{\partial n'} r' \, d\Gamma' \, d\theta \, d\theta' \\
& = \frac{-i\omega\rho}{2\pi} \int_0^{2\pi} \int_0^{2\pi} \int_{\Gamma'} v_0^{(s)}(r', z') G(\mathbf{x}, \mathbf{x}') r' \, d\Gamma' \, d\theta \, d\theta' \\
& \quad + \frac{1}{2\pi} p_0^{\text{inc}(s)}(r, z). \tag{40}
\end{aligned}$$

Since the angular dependence in the above integrals comes as the difference of the angles in the Green's function

$$G(\mathbf{x}, \mathbf{x}') = \frac{e^{ik|\mathbf{x}-\mathbf{x}'|}}{4\pi|\mathbf{x}-\mathbf{x}'|} \tag{41}$$

and

$$|\mathbf{x}-\mathbf{x}'| = \sqrt{r^2 + r'^2 - 2rr' \cos(\theta - \theta') + (z - z')^2}, \tag{42}$$

by a change of variables one of the integrals can be integrated to give  $2\pi$  and we have

$$\begin{aligned}
& \frac{1}{2} p_0^{(s)}(r, z) - \int_{\Gamma'} \int_0^{2\pi} p_0^{(s)}(r', z') \frac{\partial G(\mathbf{x}, \mathbf{x}')}{\partial n'} \, d\beta' r' \, d\Gamma' \\
& = -i\omega\rho \int_{\Gamma'} \int_0^{2\pi} v_0^{(s)}(r', z') G(\mathbf{x}, \mathbf{x}') \, d\beta' r' \, d\Gamma' \\
& \quad + \frac{1}{2\pi} p_0^{\text{inc}(s)}(r, z). \tag{43}
\end{aligned}$$

For  $m \neq 0$ , the same properties of the free space Green's function results in no contribution from terms containing the sum of the angles and in

$$\begin{aligned}
& \int_0^{2\pi} \int_0^{2\pi} G(\mathbf{x}, \mathbf{x}') \cos m(\theta - \theta') \, d\theta \, d\theta' \\
& = 2\pi \int_0^{2\pi} G(\mathbf{x}, \mathbf{x}') \cos m\beta' \, d\beta', \tag{44}
\end{aligned}$$

in terms containing the difference of the angles. Then Eq. (37) is reduced to

$$\begin{aligned}
& \frac{1}{2} p_m^{(s)}(r, z) - \int_{\Gamma'} \int_0^{2\pi} p_m^{(s)}(r', z') \cos m\beta' \frac{\partial G(\mathbf{x}, \mathbf{x}')}{\partial n'} \, d\beta' r' \, d\Gamma' \\
& = -i\omega\rho \int_{\Gamma'} \int_0^{2\pi} v_m^{(s)}(r', z') \cos m\beta' G(\mathbf{x}, \mathbf{x}') \, d\beta' r' \, d\Gamma' \\
& \quad + \frac{1}{\pi} p_m^{\text{inc}(s)}(r, z). \tag{45}
\end{aligned}$$

Defining

$$\begin{aligned}
g_m^{(s)}(r, z; r', z') &= \int_0^{2\pi} G(\mathbf{x}, \mathbf{x}') \cos m\beta' \, d\beta', \\
h_m^{(s)}(r, z; r', z') &= \int_0^{2\pi} \frac{\partial G(\mathbf{x}, \mathbf{x}')}{\partial n'} \cos m\beta' \, d\beta', \tag{46}
\end{aligned}$$

we obtain the boundary element integral equation for the symmetric circumferential coefficients for all  $m$ ,

$$\begin{aligned}
& \frac{1}{2} p_m^{(s)}(r, z) - \int_{\Gamma'} p_m^{(s)}(r', z') h_m^{(s)}(r, z; r', z') r' \, d\Gamma' \\
& = -i\omega\rho \int_{\Gamma'} v_m^{(s)}(r', z') g_m^{(s)}(r, z; r', z') r' \, d\Gamma' \\
& \quad + \frac{1}{\epsilon\pi} p_m^{\text{inc}(s)}(r, z). \tag{47}
\end{aligned}$$

Next, applying the integral operator,  $m \neq 0$ ,

$$\int_0^{2\pi} \sin m\theta \, d\theta, \tag{48}$$

to Eq. (34) gives the boundary element integral equation for the antisymmetric circumferential coefficients for all  $m > 0$ ,

$$\begin{aligned} \frac{1}{2}p_m^{(a)}(r, z) - \int_{\Gamma'} p_m^{(a)}(r', z') h_m^{(a)}(r, z; r', z') r' d\Gamma' \\ = -i\omega\rho \int_{\Gamma'} v_m^{(a)}(r', z') g_m^{(a)}(r, z; r', z') r' d\Gamma' \\ + \frac{1}{\pi} p_m^{\text{inc}(a)}(r, z), \end{aligned} \quad (49)$$

where

$$p_m^{\text{inc}(a)}(r, z) = \int_0^{2\pi} p_{\text{inc}}(\mathbf{x}) \sin m\theta d\theta \quad (50)$$

and

$$\begin{aligned} g_m^{(s)}(r, z; r', z') &= g_m^{(a)}(r, z; r', z'), \\ h_m^{(s)}(r, z; r', z') &= h_m^{(a)}(r, z; r', z'). \end{aligned} \quad (51)$$

For both the symmetric and antisymmetric circumferential orders, Eqs. (47) and (49) can be written as

$$\mathbf{A}_\ell^{(s,a)} \mathbf{P}_\ell^{(s,a)} = \mathbf{B}_\ell \mathbf{V}_\ell^{(s,a)} + \mathbf{P}_{\ell, \text{inc}}^{(s,a)}, \quad (52)$$

where the components of matrices  $\mathbf{A}_\ell^{(s,a)}$  and  $\mathbf{B}_\ell^{(s,a)}$  are given by

$$A_\ell^{(s,a)}(m, n) = \frac{1}{2} \delta_{mn} - \int_{\Gamma'} h_\ell^{(s,a)}(r_m, z_m; r'_n, z'_n) r'_n d\Gamma' \quad (53)$$

and

$$B_\ell^{(s,a)}(m, n) = -i\omega\rho \int_{\Gamma'} g_\ell^{(s,a)}(r_m, z_m; r'_n, z'_n) r'_n d\Gamma'. \quad (54)$$

Substituting Eq. (32) into Eq. (52) gives the following system of complex linear algebraic equations for each circumferential Fourier mode  $\ell$ :

$$\begin{aligned} \left[ \mathbf{A}_\ell^{(s,a)} - i\omega \mathbf{B}_\ell^{(s,a)} \mathbf{D}^{-1} \mathbf{L}_\ell^T \right. \\ \left. \times (-\omega^2 \mathbf{M}_\ell^{(s,a)} + \mathbf{K}_\ell^{(s,a)})^{-1} \mathbf{L}_\ell \right] \mathbf{P}_\ell^{(s,a)} = \mathbf{P}_{\ell, \text{inc}}^{(s,a)}. \end{aligned} \quad (55)$$

These equations are the counterparts of Eq. (A19) for an axially-symmetric scatterer ensonified by a 3D incident field obtained using the Fourier expansion in the circumferential direction. The circumferential components of normal velocity can be computed using Eq. (32), which can be used to compute the circumferential components of the scattered pressure field at the receiver,  $\mathbf{x}_r$ , using the Helmholtz-Kirchhoff integral

$$\begin{aligned} p_m^{(s,a)}(r_r, z_r) = \int_{\Gamma'} p_m^{(s,a)}(r', z') h_m^{(s,a)}(r_r, z_r; r', z') r' d\Gamma' \\ - i\omega\rho \int_{\Gamma'} v_m^{(s,a)}(r', z') g_m^{(s,a)}(r_r, z_r; r', z') r' d\Gamma', \end{aligned} \quad (56)$$

and finally the above pressure components can be used to compute the total scattered field at the receiver using Eq. (25).

It should be pointed out that the axially-symmetric boundary integral equations, like any boundary integral formulation of the Helmholtz equation, suffer from the well-known non-uniqueness problem at certain frequencies associated with the eigenfrequencies of the interior problem. This problem has no physical significance but arises as a mathematical artifact by the very process of reducing the exterior domain to the boundary. Detailed discussions of the mathematical aspects of this problem can be found in the works of Smithies,<sup>15</sup> Kleinman and Roach,<sup>16</sup> and Burton<sup>17</sup> among others. Methods of overcoming the non-uniqueness problem have been discussed by Schenck<sup>18</sup> and Burton and Miller.<sup>19</sup> In this paper we use the Combined Helmholtz Integral Equation Formulation (CHIEF) proposed by Schenck.<sup>18</sup>

#### IV. VALIDATION

In this section, we validate the method for a solid steel sphere, an aluminum spherical shell, and an acoustically soft and hard semi-sphere on an infinite plane, all of which have analytic solutions. Then to demonstrate the speed of the model, we compute the backscattered target strength as a function of aspect angle and frequency for an aluminum cylinder and compare the results to those obtained from a finite element model designed for axially-symmetric targets.<sup>14</sup> The properties of the targets used in validating the model are listed in Table I.

For an axially-symmetric target, we only need to mesh the generating planar section that, when rotated around its axis of symmetry, produces the target. In the case of a solid sphere, this would be a semicircle, with its diameter as the axis of symmetry. For the solid steel sphere, we meshed the generating semicircle by 5354 quadrilateral elements. This is equivalent to 15 elements per wavelength at the maximum frequency of 10 kHz.

The scattered pressure for an incident wave  $\vec{k}$  and in the direction  $\vec{q}$  is denoted by  $p(\vec{k}, \vec{q})$ , which can be computed using Eq. (25). We computed the backscattering amplitude,  $T = p(\vec{k}, -\vec{k})$ , as a function of frequency, ranging from 0 to 10 kHz. The results for the solid steel sphere are shown in Fig. 2, where the solution is compared with the classical partial wave solution<sup>20</sup> for a plane wave.

A comparison of the backscattering scattering amplitude,  $T$ , also for a plane wave, from an empty aluminum spherical shell for the same frequency range, computed using our method and the partial wave method<sup>20</sup> is shown in Fig. 3. The radius of the sphere is 0.5 m and the shell thickness is 5 cm. The generating planar section, which in this case is a 5-cm wide, semi-circular strip was meshed using 5811 quadrilateral

TABLE I. The properties of the targets used in validating the model.  $r$  is the radius,  $\Delta$  is the shell thickness,  $L$  is the length,  $E$  is the Young's modulus,  $\rho$  is the density, and  $\nu$  is the Poisson ratio.

Target	$r$ (m)	$\Delta$ (cm)	$L$ (m)	$E$ (Pa)	$\rho$ (kg/m <sup>3</sup> )	$\nu$
Solid steel sphere	0.5	N/A	N/A	$2.05 \times 10^{11}$	7850	0.28
Aluminum spherical shell	0.5	5	N/A	$72.3 \times 10^9$	2700	0.35
Hemispherical boss	0.5	N/A	N/A	N/A	N/A	N/A
Solid aluminum cylinder	0.1524	N/A	0.6096	$72.3 \times 10^9$	2700	0.35

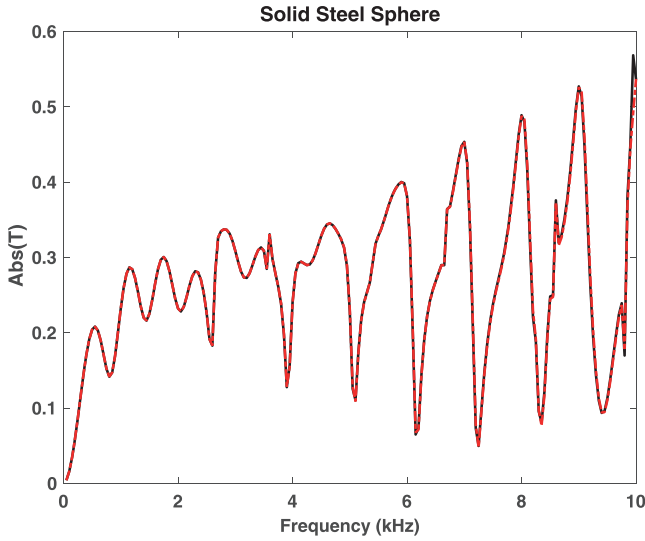


FIG. 2. (Color online) The backscattering amplitude as a function of frequency for a solid steel sphere of radius 0.5 m. The solid black line represents the partial wave solution and the red dashed-dotted line represents the coupled finite-boundary element solution. The frequency step is 50 Hz.

elements (40 elements per wavelength at the maximum frequency of 10 kHz). In both cases, there is excellent agreement between our solutions and the benchmark solutions. The Green's function used in the above two cases is the free space Green's function given by Eq. (41). Another class of problems with a slightly more complicated Green's function, which also lends itself to an analytical solution, is the case of an acoustically soft or rigid hemisphere on an infinite plane satisfying the same boundary conditions. This is also referred to as an infinite plane with a hemispherical boss. The analytical solution is obtained from the partial wave solution referenced above using the method of images by forming solutions for an incident field and an image incident field. Since each solution satisfies the boundary condition on the surface of the sphere, their superposition can be used to enforce the same boundary

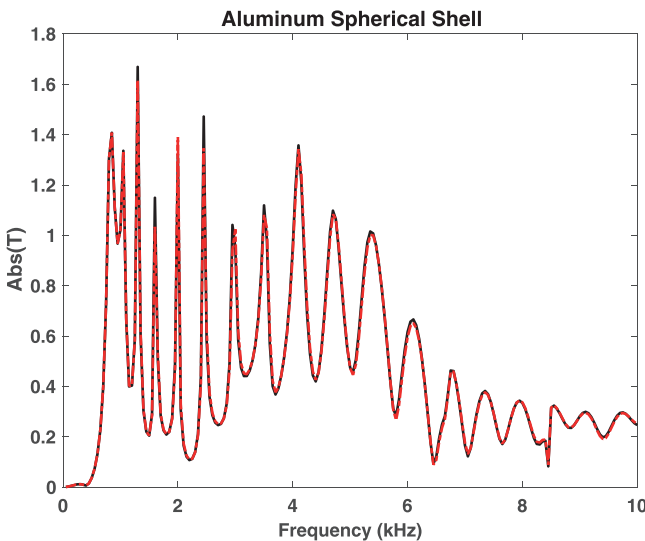


FIG. 3. (Color online) The backscattering amplitude as a function of frequency for a 0.5 m, empty, aluminum spherical shell. The solid black line represents the partial wave solution and the red dashed-dotted line represents the coupled finite-boundary element solution. The frequency step is 50 Hz.

condition on the surface of symmetry and thus the entire surface of interest. A similar procedure is used to compute scattering for a hemispherical boss using our model. The Green's function used in our formulation for the acoustically soft case with the infinite plane at  $z = 0$  is

$$G_D(r, z, \theta; r', z', \theta') = G_1 - G_2, \quad (57)$$

where

$$G_1(r, z, \theta; r', z', \theta') = \frac{e^{ik\sqrt{r^2+r'^2-2rr'\cos(\theta-\theta')+(z-z')^2}}}{4\pi\sqrt{r^2+r'^2-2rr'\cos(\theta-\theta')+(z-z')^2}},$$

$$G_2(r, z, \theta; r', z', \theta') = \frac{e^{ik\sqrt{r^2+r'^2-2rr'\cos(\theta-\theta')+(z+z')^2}}}{4\pi\sqrt{r^2+r'^2-2rr'\cos(\theta-\theta')+(z+z')^2}}. \quad (58)$$

For the rigid case the Green's function is given by

$$G_N(r, z, \theta; r', z', \theta') = G_1 + G_2. \quad (59)$$

These Green's functions guarantee that the total field vanishes on the infinite plane for the acoustically soft case and its normal derivative vanishes on the same surface for the acoustically hard case. The BEM then enforces the same boundary conditions on the surface of the hemispherical boss, resulting in a self-consistent solution. In this example, the radius of the hemispherical boss is 0.5 m and the problem is solved for a plane wave making a  $30^\circ$  angle with the positive  $x$  axis for two frequencies of 5 and 10 kHz. The scattered field is computed as a function of the receiver angle. The problem is solved using ten Fourier circumferential orders. Since for the above boundary conditions the surface is non-penetrable, this is only a boundary element problem. Hence, the scattering is purely geometrical and is caused by a surface whose cross section is shown in the inset in Fig. 4. The quarter-circle generating curve produced the surface of the hemispherical boss by revolving around a diameter perpendicular to the infinite plane (see the inset in Fig. 4). This curve was meshed by 158 linear elements. The boundary conditions (acoustically soft or hard) on the infinite plane are enforced by the Green's functions defined by Eqs. (57) and (59) and on the surface of the hemisphere by the scattering model. The solutions are shown in Fig. 4, where they are compared with the corresponding exact partial wave solutions.

To demonstrate the speed of the model, we next compute the backscattering target strength as a function of aspect angle and frequency for an aluminum cylinder in free space. The radius of the cylinder is 0.5 ft, its height is 2.0 ft, and the incident field is a plane wave. The generating plane in this case is a  $2 \times 0.5$  ft rectangle, which was meshed by 900 quadrilateral elements (15 elements per wavelength at 10 kHz). We used 10 circumferential orders in the axially-symmetric solution with 100 Hz frequency steps from 1 to 10 kHz and  $1^\circ$  angular steps from  $0^\circ$  to  $90^\circ$ . The results are

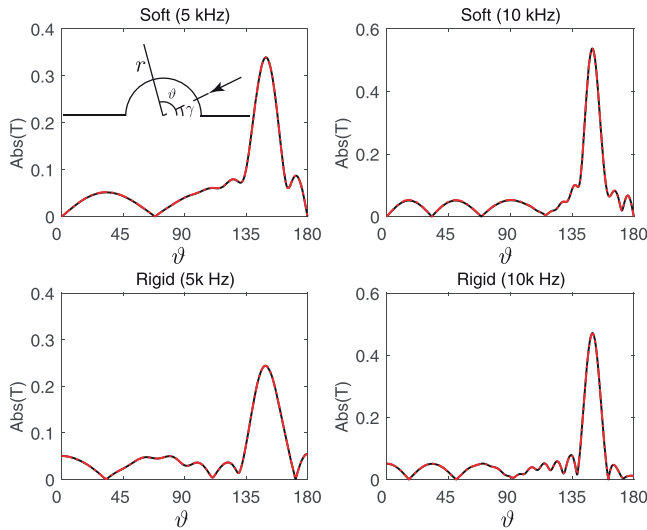


FIG. 4. (Color online) The scattering amplitude as a function of the receiver angle for a hemispherical boss. The scattering geometry is shown in the inset in the top left panel. The incident plane wave makes an angle  $\gamma = 30^\circ$  with the  $x$  axis in all cases. The receiver angle,  $\vartheta$  varies from zero to  $180^\circ$ . The top and bottom panels show the results for the acoustically soft and rigid cases, respectively. The left and right panels are for the incident frequency of 5 and 10 kHz. The solid black line represents the partial wave solution and the red dashed-dotted line represents the coupled finite-boundary element solution.

shown in Fig. 5, where the figure on the left is obtained using Axi-Scat developed by Zampolli *et al.*<sup>14</sup> The latter is an axially-symmetric model that solves the problem by using the axially-symmetric module in COMSOL (Ref. 21) for each circumferential order and then performs a Fourier sum for each frequency and aspect angle. The small differences between the two solutions can be due to differences in discretization, numerical computation of integrals, the types of basis functions used, and other factors. Furthermore, Axi-Scat uses Perfectly Matched Layers (PMLs) to prevent reflections from the boundaries of the computational domain. If the PML is not implemented properly, superfluous reflections can occur, and sometimes they cannot be eliminated entirely. Our solution, being a boundary element solution, does not use a PML. It is usually difficult to ensure that all the above parameters are the same, so small differences are bound to occur. We made sure that both solutions have converged by reducing the mesh size and increasing the number of circumferential orders until the solution stabilized. Usually, a mesh size of 15 elements per wavelength at the highest frequency and a maximum circumferential order of 10 are adequate. The same parameters can affect the Axi-Scat solution and we made sure that both numbers were adequate.

In our computations, COMSOL was not used. Instead we used the equations developed in Sec. II to compute scattering from an elastic structure and the equations developed in Sec. III to compute the acoustic field at the receiver.<sup>22</sup> We ran both models on a Mac Pro with 12 processors. The Axi-Scat solution took 12h to run, and in contrast our axially-symmetric model only took 19min to run. One of the reasons why our model is so much faster is that it solves a boundary element problem with fewer number of unknowns.

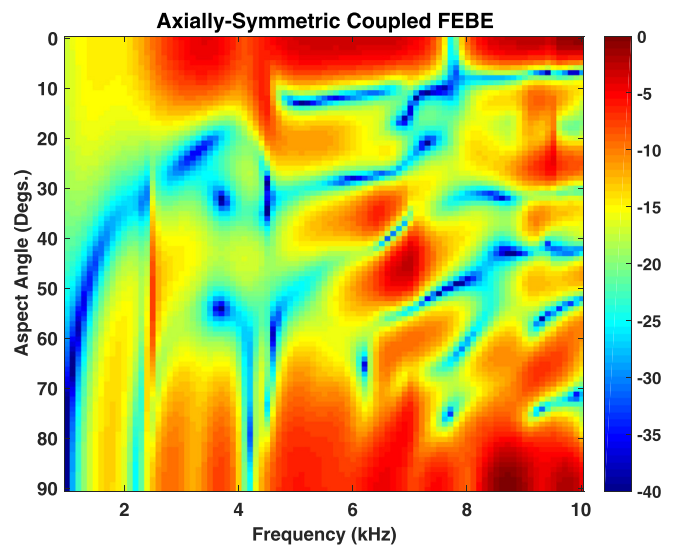
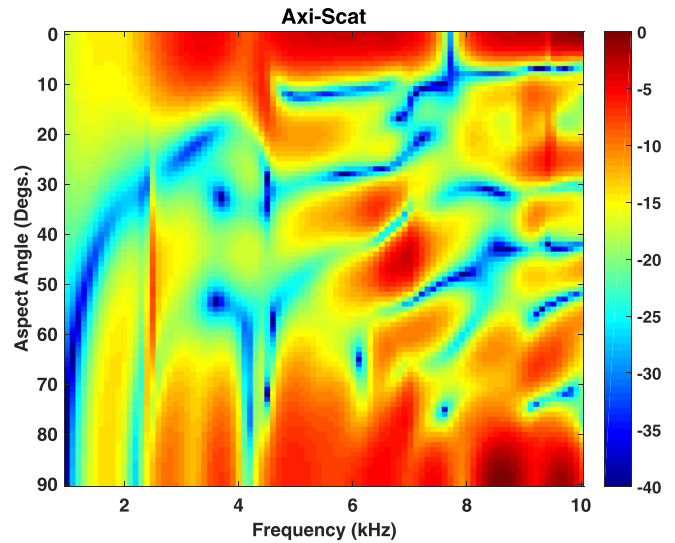


FIG. 5. (Color online) The backscattering target strength for a 1-ft by 2-ft aluminum cylinder as a function aspect angle and frequency. Zero degree and  $90^\circ$  correspond to backscattering from broadside and end-fire, respectively. The figure on the left was produced by the Axi-Scat model and the one on the right by the model derived in this paper.

The other reason is that in computing the scattered field we only invert Eq. (55) for each frequency, but not for each aspect angle since the incident field is on the right-hand side. In comparison, Axi-Scat solves an axially-symmetric finite element problem for each frequency, aspect angle, and circumferential order.

## V. SUMMARY AND CONCLUSIONS

In this paper we used the fluid-structure interaction method to develop a technique to compute scattering from axially-symmetric elastic structures in three dimensions, i.e., ensonified by a non-axially-symmetric field in free space. The fluid-structure interaction method is based on formulating the equations of motion in the structure using the finite element method and formulating the sound propagation in the surrounding environment using the boundary integral method. The two methods are self-consistently coupled by

imposing the continuity of pressure and normal particle velocity on the surface of the structure. This method combines the accuracy of the finite element method to model the elastic structure and the robustness of the BEM to model the acoustic field in the surrounding fluid environment to produce a numerically accurate and self-consistent solution. The axially-symmetric nature of the structure allows the use of a Fourier expansion in the circumferential direction to enable the model to compute scattering from objects exposed to 3D (non-axially-symmetric) incident fields. This method essentially reduces a 3D problem to a series of 2D problems, one for each circumferential order, delivering significant reductions in computation time.

The model was validated using three analytical solutions and an axially-symmetric finite element solution (Axi-Scat). The latter was used to compute the backscattering target strength as a function of frequency and aspect angle for a finite aluminum cylinder. A comparison between our solution and that of Axi-Scat shows that our model is more than 36 times faster. A derivation of the fluid-structure formulation for an arbitrary structure is provided in the [Appendix](#).

## ACKNOWLEDGMENTS

This work was supported by the Strategic Environmental Research and Development Program (SERDP) Contract No. W912HQ-14-C-0010 and ONR Contract No. N00014-00-D-0115 in support of the Effects of Sound on the Marine Environment program. We would also like to thank the two anonymous reviewers for their careful review of our paper and for their useful and constructive comments.

## APPENDIX: FLUID-STRUCTURE FORMULATION FOR AN ARBITRARY STRUCTURE

The scattered field from a structure for an incident field,  $p_{\text{inc}}(\mathbf{x})$ , is given by Eq. (33), where  $G(\mathbf{x}, \mathbf{x}')$  represents the Green's function for any environment in which the scattering takes place.

In Eq. (33) there are two unknown quantities, the pressure  $p$  and the surface normal velocity  $v_n$ . Consequently, an additional equation is needed. The requisite second equation is provided by the weighted-residual formulation of the steady-state vibration of a solid structure. We assume that body forces are absent and the vibrating solid is free of displacement constraints, i.e., the solid is free-floating in the acoustic medium. The weak formulation of the governing equations then results in the Galerkin weighted residual equation Eq. (10),

$$-\omega^2 \int_{D_-} \delta \mathbf{u}^T \rho \mathbf{u} dV + \int_{D_-} \delta \mathbf{u}^T \mathcal{B}^T \mathbf{D} \mathcal{B} \mathbf{u} dV + \int_S \delta \mathbf{u}^T \mathbf{p} n dS = 0. \quad (\text{A1})$$

Here  $V = V_-$  and  $S$  are the solid domain volume and boundary surface, respectively,  $\mathbf{u}$  is the displacement,  $\mathbf{D}$  is the  $6 \times 6$  material stiffness matrix defined in Eq. (17), and  $\mathcal{B}$  is the symmetric gradient operator that generates the symmetrized

small-deformation gradient tensor components, including a factor of 2 required for the shear components in the present ‘‘Voigt’’ vector formulation

$$\mathcal{B} = \begin{bmatrix} \partial/\partial x & 0 & 0 \\ 0 & \partial/\partial y & 0 \\ 0 & 0 & \partial/\partial z \\ \partial/\partial y & \partial/\partial x & 0 \\ \partial/\partial z & 0 & \partial/\partial x \\ 0 & \partial/\partial z & \partial/\partial y \end{bmatrix}. \quad (\text{A2})$$

Both the displacements of the solid  $\mathbf{u}$  in  $D_-$  and the distribution of the total pressure  $p$  in the surrounding medium are unknown. To produce a closed system of coupled equations, the relationship between velocity and displacement

$$\mathbf{u} = -i\omega \mathbf{v}, \quad (\text{A3})$$

is used in Eq. (33) and the equation of motion for the structure Eq. (A1). In this work, the continuous Galerkin method employs hexahedral eight-node elements to discretize Eq. (A1) for a solid structure. Full Gaussian quadrature is used for the dilatational part of the strain energy, and the shear energy is under-integrated with one-point Gaussian quadrature. Note that the bounding surface of the finite element model of the solid meshes the surface  $S$  with the quadrilateral faces of the hexahedral finite elements. These quadrilaterals are converted to panels over which the boundary element model establishes its discretization.

Introducing the finite element basis functions and the displacement degrees of freedom at the nodes

$$\begin{aligned} [\mathbf{u}(\mathbf{x}, t)] &= \begin{bmatrix} u_x(\mathbf{x}, t) \\ u_y(\mathbf{x}, t) \\ u_z(\mathbf{x}, t) \end{bmatrix} = \sum_{i=1}^N N_i(\mathbf{x}) [\mathbf{u}_i(t)] \\ &= \sum_{i=1}^N N_i(\mathbf{x}) \begin{bmatrix} u_{ix}(t) \\ u_{iy}(t) \\ u_{iz}(t) \end{bmatrix}, \end{aligned} \quad (\text{A4})$$

Eq. (A1) is converted to the complex algebraic equation

$$(-\omega^2 \mathbf{M} + \mathbf{K}) \mathbf{U} = \mathbf{F}, \quad (\text{A5})$$

where the mass and stiffness matrices consist of  $3 \times 3$  submatrices coupling nodes  $i$  and  $k$ : the mass matrix

$$\mathbf{M}_{ik} = \begin{bmatrix} 1 & 0 & 0 \\ 0 & 1 & 0 \\ 0 & 0 & 1 \end{bmatrix} \int_{V_-} N_i \rho N_k dV_- \quad (\text{A6})$$

and the stiffness matrix

$$\mathbf{K}_{ij} = \int_{V_-} [\mathcal{B} N_i]^T \mathbf{D} [\mathcal{B} N_j] dV_- \quad (\text{A7})$$

In the above,  $\mathbf{U}$  is the vector of the displacement degrees of freedom, and the vector of the nodal forces resulting from the impinging acoustic wave loading consists of  $3 \times 1$  matrices

$$\mathbf{F}_k = - \int_S p \mathbf{n} N_k dS \quad (\text{A8})$$

for each node  $k$ .

The middle equation in Eq. (33) can be written

$$\begin{aligned} \frac{1}{2} p(\mathbf{x}) - \int p(\mathbf{x}') \frac{\partial G(\mathbf{x}, \mathbf{x}')}{\partial n} dS' \\ = -i\omega\rho \int v_n(\mathbf{x}') G(\mathbf{x}, \mathbf{x}') dS' + p_{\text{inc}}(\mathbf{x}), \quad x \in S. \end{aligned} \quad (\text{A9})$$

To discretize the above, we expand both  $p$  and  $v_n$  in a linear combination using basis functions  $\phi_i$  that are piecewise constant over each of the quadrilateral panels of the tiling of the surface

$$p(\mathbf{x}) = \sum_{i=1}^N p_i \phi_i(\mathbf{x}), \quad v_n(\mathbf{x}) = \sum_{i=1}^N v_{n,i} \phi_i(\mathbf{x}). \quad (\text{A10})$$

Each of the quadrilateral panels corresponds to a face of the hexahedral element employed for the solid scatterer that is exposed to the acoustic medium.

Substituting Eq. (A10) into Eq. (A9) results in

$$\mathbf{A}\mathbf{P} = \mathbf{B}\mathbf{V}_n + \mathbf{P}_{\text{inc}}, \quad (\text{A11})$$

where

$$\begin{aligned} A_{ij} &= \frac{\delta_{ij}}{2} - \int_{s_j} \phi_j(\mathbf{x}') \frac{\partial G(\mathbf{x}_i, \mathbf{x}')}{\partial n'} dS', \\ B_{ij} &= -i\omega\rho \int_{s_j} \phi_j(\mathbf{x}') G(\mathbf{x}_i, \mathbf{y}') dS', \end{aligned} \quad (\text{A12})$$

where in this paper we use Gaussian quadrature to evaluate the above integrals. Both integrands in Eq. (A12) possess integrable singularities when  $\mathbf{x} \rightarrow \mathbf{x}'$ , which can be handled by a variety of methods (see Colton *et al.*,<sup>23</sup> Burton,<sup>17</sup> and the references therein). In this paper we employ the method used by Everstine and Henderson.<sup>24</sup>

The finite and boundary element models are coupled in the discrete form. The discrete equations for the finite element model are given by Eq. (A5). The vector  $\mathbf{F}$  reflects the loading of the scatterer by the total pressure on its surface. Approximating the distribution of the total pressure on the surface using Eq. (A10), where positive hydrodynamic pressure generates force acting against the outer normal to the solid surface, allows us to write

$$\mathbf{F} = -\mathbf{L}\mathbf{P}, \quad (\text{A13})$$

where  $\mathbf{L}$  is a rectangular coupling matrix defined in components as

$$L_{(K,j)m} = \int_{S_m} N_K(\mathbf{x}) n_j dS, \quad (\text{A14})$$

with the notation  $(K, j)$  indicating a map from node number  $K$  and coordinate direction  $j$  to a degree of freedom number  $(K, j)$ ;  $m$  is the pressure degree of freedom in the BEM,  $S_m$  is the surface element  $m$ , and  $\mathbf{P}$  is the vector of pressure values on the surface panels.

Analogously, the mean normal velocity in the boundary element model, piecewise constant along the surface panels, can be expressed from the vector of the nodal velocities of the scatterer finite element model as

$$\mathbf{V}_n = \mathbf{D}^{-1} \mathbf{L}^T \mathbf{V}, \quad (\text{A15})$$

where  $\mathbf{D}$  is a diagonal matrix of surface panel areas,

$$D_{mm} = \int_{S_m} dS, \quad (\text{A16})$$

so that, using the expression for the vector of nodal velocities,  $\mathbf{V} = -i\omega\mathbf{U}$ ,

$$\mathbf{V}_n = -i\omega\mathbf{D}^{-1} \mathbf{L}^T \mathbf{U}. \quad (\text{A17})$$

Consequently, combining Eqs. (A17), (A5), (A13), and (A11) yields

$$\begin{aligned} \mathbf{A}\mathbf{P} &= \mathbf{B}\mathbf{V}_n + \mathbf{P}_{\text{inc}} \\ &= -i\omega\mathbf{B}\mathbf{D}^{-1} \mathbf{L}^T \mathbf{U} + \mathbf{P}_{\text{inc}} \\ &= i\omega\mathbf{B}\mathbf{D}^{-1} \mathbf{L}^T (-\omega^2\mathbf{M} + \mathbf{K})^{-1} \mathbf{L}\mathbf{P} + \mathbf{P}_{\text{inc}}, \end{aligned} \quad (\text{A18})$$

or

$$\left[ \mathbf{A} - i\omega\mathbf{B}\mathbf{D}^{-1} \mathbf{L}^T (-\omega^2\mathbf{M} + \mathbf{K})^{-1} \mathbf{L} \right] \mathbf{P} = \mathbf{P}_{\text{inc}}, \quad (\text{A19})$$

which may be solved for the panel values of total pressure  $\mathbf{P}$ . Having computed  $\mathbf{P}$ , the normal velocity can be computed from Eq. (A18),

$$\mathbf{V}_n = i\omega\mathbf{D}^{-1} \mathbf{L}^T (-\omega^2\mathbf{M} + \mathbf{K})^{-1} \mathbf{L}\mathbf{P}. \quad (\text{A20})$$

<sup>1</sup>D. T. Wilton, "Acoustic radiation and scattering from elastic structures," *Int. J. Numer. Methods Eng.* **13**, 123–138 (1978).

<sup>2</sup>A. T. Abawi, P. Krysl, A. España, S. Kargl, K. Williams, and D. Plotnick, "Modeling the acoustic response of elastic targets in a layered medium using the coupled finite element/boundary element method," *J. Acoust. Soc. Am.* **140**(4), 2968 (2016).

<sup>3</sup>S. Amini, P. J. Harris, and D. T. Wilton, in *Coupled Boundary and Finite Element Methods for the Solution of the Dynamic Fluid-Structure Interaction Problem* (Springer-Verlag, New York, 1992), Chaps. 2 and 4.

<sup>4</sup>N. Atalla and F. Sgard, *Finite Element and Boundary Methods in Structural Acoustics and Vibration* (CRC Press, Boca Raton, FL, 2015).

<sup>5</sup>A. T. Abawi and P. Krysl, "The fluid-structure interaction technique specialized to axially symmetric targets," *J. Acoust. Soc. Am.* **136**(4), 2086 (2014).

<sup>6</sup>E. L. Wilson, "Structural analysis of axisymmetric solids," *AIAA J.* **3**(12), 2269–2274 (1965).

<sup>7</sup>O. C. Zienkiewicz, *The Finite Element Method*, 3rd ed. (McGraw-Hill, New York, 1977).

<sup>8</sup>L. A. Winnicki and O. C. Zienkiewicz, "Plastic (or viscoplastic) behavior of axisymmetric-bodies subjected to non-symmetric loading semi-analytical finite-element solution," *Int. J. Numer. Methods Eng.* **14**(9), 1399–1412 (1979).

<sup>9</sup>R. L. Spilker and D. M. Dugirda, "Analysis of axisymmetric structures under arbitrary loading using the hybrid-stress model," *Int. J. Numer. Methods Eng.* **17**(6), 801–828 (1981).

<sup>10</sup>J. P. Carter and J. R. Booker, "Consolidation of axi-symmetric bodies subjected to non axi-symmetric loading," *Int. J. Numer. Anal. Methods Geomech.* **7**(2), 273–281 (1983).

<sup>11</sup>K. T. Danielson and J. T. Tielking, "Fourier continuum finite-elements for large-deformation problems," *Comput. Struct.* **49**(1), 133–147 (1993).

- <sup>12</sup>T. M. V. Kaiser, A. E. Elwi, and A. Mioduchowski, "Large-displacement axisymmetrical element for nonaxisymmetric deformation," *AIAA J.* **31**(11), 2186–2188 (1993).
- <sup>13</sup>V. N. Kukudzhanov and D. N. Shneiderman, "Solution of elastoplastic problems of the non-axially symmetric deformation of bodies of revolution," *J. Appl. Math. Mech.* **61**(3), 503–11 (1997).
- <sup>14</sup>M. Zampolli, A. Tesei, F. B. Jensen, N. Malm, and J. B. Blottman III, "A computationally efficient finite element model with perfectly matched layers applied to scattering from axially symmetric objects," *J. Acoust. Soc. Am.* **122**(3), 1472–1485 (2007).
- <sup>15</sup>F. Smithies, *Integral Equations* (Cambridge University Press, Cambridge, England, 1958), pp. 160–172.
- <sup>16</sup>R. E. Kleinman and G. F. Roach, "Boundary integral equations for the three dimensional Helmholtz equation," *SIAM Rev.* **16**, 214–236 (1974).
- <sup>17</sup>A. J. Burton, in "The solution of Helmholtz equation in exterior domains using integral equations," NPL Report NAC 90, National Physical Laboratory Teddington, Middlesex, United Kingdom (1973).
- <sup>18</sup>H. A. Schenck, "Improved integral formulation for acoustic radiation problems," *J. Acoust. Soc. Am.* **44**(1), 41–58 (1968).
- <sup>19</sup>A. J. Burton and G. F. Miller, "The application of integral equation methods to the numerical solutions of some exterior boundary value problems," *Proc. R. Soc. London Ser. A* **323**, 201–210 (1971).
- <sup>20</sup>R. R. Goodman and R. Stern, "Reflection and transmission of sound by elastic spherical shells," *J. Acoust. Soc. Am.* **34**(3), 338–344 (1962).
- <sup>21</sup>COMSOL Multiphysics 3.5a User's Guide (2009), COMSOL AB, Stockholm (2009).
- <sup>22</sup>P. Krysl, FAESOR: Matlab object-oriented Finite Element toolkit, <http://hogwarts.ucsd.edu/~pkrysl/faesor>, 2008–2017 (Last viewed November 1, 2017).
- <sup>23</sup>D. Colton and R. Kress, in *Integral Equation Methods in Scattering Theory* (John Wiley and Sons, New York, 1983).
- <sup>24</sup>G. C. Everstine and F. M. Henderson, "Coupled finite element/boundary element approach for fluid-structure interaction," *J. Acoust. Soc. Am.* **87**(5), 1938–1947 (1990).